Progress In Electromagnetics Research, PIER 98, 1–13, 2009

A WIDEBAND HALF OVAL PATCH ANTENNA FOR BREAST IMAGING

J. Yu †, **M. Yuan**, **and Q. H. Liu**

Department of Electrical and Computer Engineering
Duke University
Durham, NC 27708, USA

Abstract—A simple half oval patch antenna is proposed for the active breast cancer imaging over a wide bandwidth. The antenna consists of a half oval and a trapezium, with a total length 15.1 mm and is fed by a coaxial cable. The antenna performance is simulated and measured as immersed in a dielectric matching medium. Measurement and simulation results show that it can obtain a return loss less than −10 dB from 2.7 to 5 GHz. The scattered field detection capability is also studied by simulations of two opposite placed antennas and a full antenna array on a cubic chamber.

1. INTRODUCTION

Breast cancer is the most common cancer in women, but fortunately early detection and treatment can significantly improve the survival rate. Ultrasound, mammography and magnetic resonance imaging (MRI) are currently used clinically for breast cancer diagnosis [1]. However, these techniques have many limitations, such as high rate of missed detections, ionizing radiation (mamography), too expensive to be widely available, and so on. Compared with conventional mammography, microwave imaging of breast tumors is a nonionizing, potentially low-cost, comfortable and safe alternative [2]. The high contrast of the dielectric property between the malignant tumor and the normal breast tissue should manifest itself in terms of lower numbers of missed detections and false positives [3, 4]. The microwave breast tumor detection also has the potential to be both sensitive and specific, to detect small tumors, and to be less expensive than methods such as MRI.

Corresponding author: M. Yuan (mengqing.yuan@duke.edu).
† Also with National Key Laboratory of EMC, Wuhan, Hubei 430064, China.

Theoretical analysis and numerical simulation results have shown that microwave imaging for breast cancer is feasible [5–13], but during practical fabrication of imaging systems, there are many practical problems [14]. One of the biggest challenges of constructing a microwave breast cancer imaging system is the sensor design. Various types of antennas have been proposed by research groups involved in breast cancer detection applications [15–20]. For example, [16] proposed and fabricated a compact stair-shaped dielectric resonator antenna (DRA) for microwave breast cancer detection. A quarter-wavelength choke was incorporated to reduce the finite ground plane size. [17] studied and compared the detection capabilities of two co-polarized and cross-polarized antenna arrays consisting of two slot, CPW fed antennas for the purpose of ultra-wideband breast cancer detection. [18] proposed an antenna for radar-based breast imaging, which detects tumors by observing variations in microwave signals reflected from the tumors as the antenna location changes. Different breast cancer detection methods need different antennas. Most antennas proposed recently are applied to the time-domain-based detection method, capable of detecting the location of tumor, but not targeted for the reconstruction of the whole breast dielectric distributions.

Here we proposed a prototype of 3D imaging system, which uses a small $100 \times 100 \times 100\,\mathrm{mm}^3$ cubic chamber integrated with patch antenna arrays [21, 22] as the sensor. One chamber can contain one breast immersed in a matching dielectric medium. And the antenna array located on four vertical walls of the chamber can sweep and acquire 3D scattered field data in a relatively short time.

For a breast imaging system, the antenna should be compact, lightweight and suitable for directly touching the breast. [21, 22] proposed a kind of bowtie patch antenna for imaging at 2.75 GHz. However, broadband antennas are preferable to increase the possibility of detecting tumors over a large range of sizes. So an operating bandwidth of 2.7–5 GHz is the objective of this work.

This paper presents a simple half oval patch antenna that can operate over the necessary wide bandwidth for this application. The half oval patch antenna presented here has been proposed to radiate directly into a dielectric medium (matching medium).

As described in subsequent sections, the initial antenna design and performance optimization were carried out by simulations with HFSS and Wavenology EM. And the performance of proposed antenna is validated by measurement. For further integration and scattered field calculation, we will study and compare the coupling of the antenna array and determine the smallest spacings for reducing interferences

among antennas. The detection capability of the antenna array will be discussed by simulations of different positions in a matching dielectric medium.

2. ANTENNA DESIGN

2.1. Half Oval Patch Antenna Structure

According to the imaging system requirement as discussed in [21, 22], the antennas will be mounted on four vertical panels of a cubic chamber. Each panels has the same number of antennas. To obtain the data for reconstruction of the breast dielectric distribution, the antennas are switched electronically between source and receiver one by one. In each scan process, only one antenna is used as the source and the others act as receivers.

We choose an oval antenna as our initial structure, then change it to half oval for reducing its size. Because the antenna size is too small to omit the coaxial connector in simulation, we proposed an trapezium for connecting the coaxial cable connector and the half oval antenna arm, which can keep the antenna in the same size but with better return loss performance. This design uses a $100 \times 100\,\mathrm{mm}^2$ FR4 substrate (1.6 mm thickness). The ground plane is placed right behind the substrate and covers the whole substrate. The antenna is fed by a coaxial line. Because each antenna is as small as 15.1 mm, the coaxial cable connector should be considered as part of the antenna design. The dimensions and structure are shown in Fig. 1. The inner conductor of the coaxial cable connector (SMB 50 Ohm connector) is modeled as a cylinder 1.27 mm in diameter. And the dielectric insulator in the connector is Teflon. The outer diameter of the cable is 4.2 mm and is connected with the ground plane. In our model, the thickness of the shell is 1 mm, which is not shown in the figure. The fabricated antenna prototype is made of copper. The thickness of patch is 0.16 mm for both simulation model and real antenna.

2.2. Antenna Performance

During the breast cancer detection and imaging, a matching medium should be applied to surround the breast to reduce the scattering from the breast skin. The relative permittivity (ε_r) of tumor varies from 40 to 60, and normal breast tissue varies from 9 to 25 [23–26]. From the past experimental experiences [21], we choose acetone as the matching medium, whose relative permittivity is $\varepsilon_r = 21.8$ and conductivity is $\sigma = 0.17\,\mathrm{S/m}$. Acetone is easy to obtain for the system prototype development.

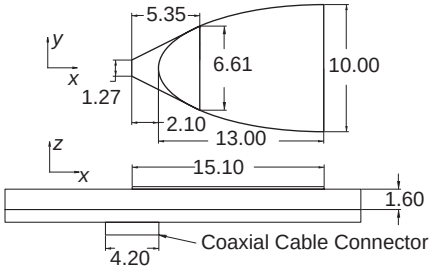

Figure 1. Top and side views of a half oval patch antenna. (Unit: mm).

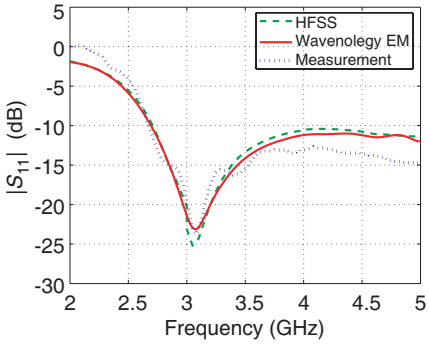

Figure 2. Return loss simulation and measurement results for the antenna in Fig. 1.

We assume that the normal breast tissue is perfectly matched with the medium. So above the patch antenna is matching medium, while it is the air under the PEC ground plane. With these design considerations, the prototype antenna shown in Fig. 1 is simulated by both HFSS and Wavenology EM. We we measured the $|S_{11}|$ parameter in acetone by an Agilent E8362B PNA series network analyzer. The simulated and measured return loss results from 2 to 5 GHz in Fig. 2 show good agreement. Both commercial software simulation results and measurement results indicate that the proposed half oval patch antenna satisfies the basic performance requirements, and the length is as short as 15.1 mm. The reflection is less than -10 dB within 2.7–5 GHz.

2.3. Array Design

An imaging system with a chamber size $100 \times 100 \times 100\,\text{mm}^3$ was proposed to fit regular breast size [21]. One prototype of the chamber is shown in Fig. 3 and Fig. 4. The vertical spacing between two adjacent antennas is defined as D_v, while the horizontal spacing is noted as D_h. In this prototype, each plane has a 3×3 antenna array. And the ground covers the 4 side and bottom panels to isolate the noise from the environment. The antennas in each array has the same vertical and horizontal spacings. How to arrange the antennas on each plane and how to choose D_v and D_h will be discussed below.

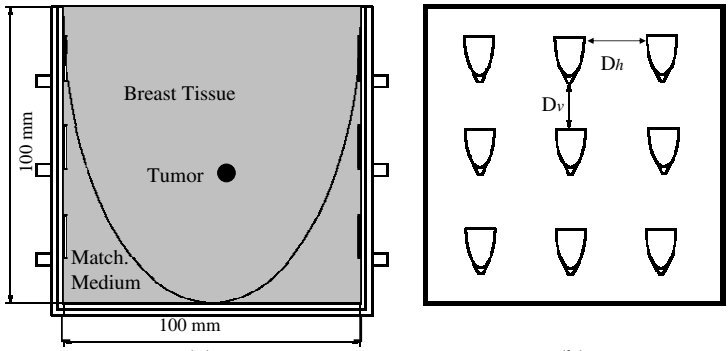

Figure 3. (a) Side view of the imaging chamber. (b) Each face of the imaging chamber with 3×3 antennas.

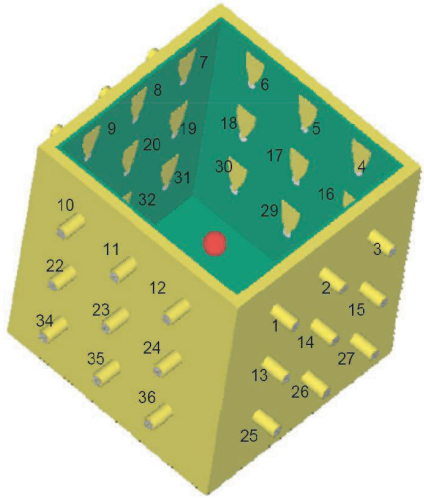

Figure 4. 3D view of the chamber with an array of 36 antennas.

3. ANTENNA COUPLING ANALYSIS

The antennas will be integrated into a 3-D array on the four vertical walls of the cubic chamber. Usually, the more antennas the wall contains, the more imaging data can be obtained from each scan, but the undesirable coupling may be stronger and the array becomes more expensive. So the spacings of the antenna array are also discussed in the paper. The couplings between the co-polarized horizontal and vertical array elements are represented by $|S_{21}|$.

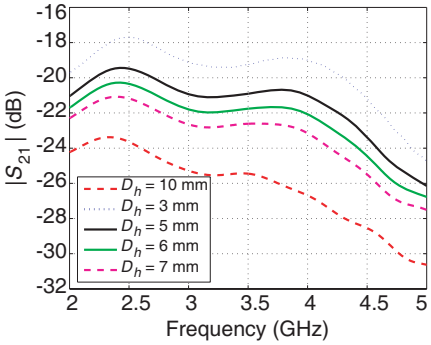

Figure 5. Coupling versus the horizontal distance of two parallel antennas.

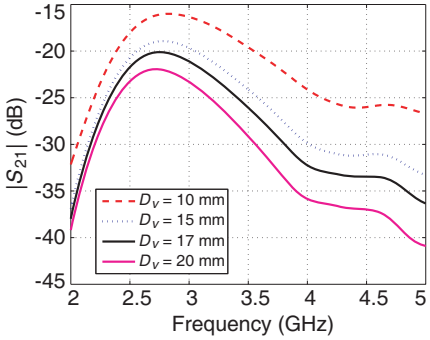

Figure 6. Coupling versus the vertical distance of two parallel antennas.

The antennas will be parallel mounted on each of the four side panels. Here, we studied the vertical (D_v) and horizontal (D_h) spacings for any two half oval patch antennas on the same plane as Fig. 3(b) shows. The simulation is under the assumption that there are only two antennas on a 100 mm $\times$100 mm substrate (ground covers the whole substrate).

According to the study of [17], we choose -20 dB as the coupling requirement in the imaging frequency band of 2.7 to 5 GHz. From the simulation results shown in Fig. 5 and Fig. 6, we can see that to meet the requirement of isolation less than -20 dB, the smallest D_h is 5 mm, while smallest D_v is 17 mm. As a preliminary study of this kind of imaging system, these results are only for the reference of further antenna array design.

4. ANTENNA DETECTION CAPABILITY

For breast cancer imaging application, the antenna should be able to detect weak signals and identify small tumors, and high quality signals received will benefit the imaging. So we place two half oval patch antennas on the opposite sides in Fig. 7 to determine the detection capability of the antennas. The space between two antennas is also filled with a homogenous dielectric material (breast tissue surrounded by matching medium, and skin is omitted here). We assume that the tumor is spherical, and located at the center point between two antennas (deepest place under skin for detection) as in Fig. 7. The relative permittivity of the tumor is $\varepsilon_r = 50$, and conductivity is $\sigma = 9$ S/m [19].

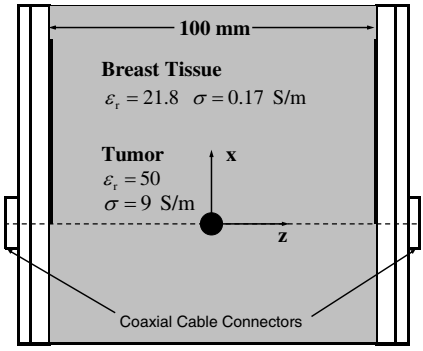

Figure 7. Placement sketch of two opposite antennas.

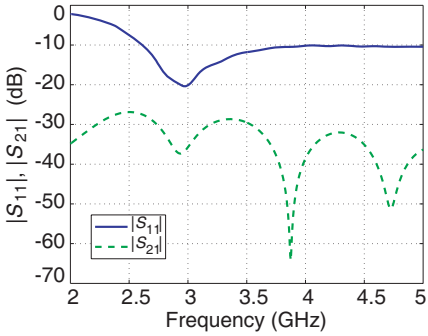

Figure 8. Simulated $|S_{11}^{inc}|$ and $|S_{21}^{inc}|$ results for the configuration in Fig. 7.

The scattered field of the tumor is calculated by subtracting the incident field (background field) from the total field. Here the incident field means the electromagnetic field generated by one antenna radiation in dielectric medium when there is no tumor, while the total filed is the corresponding field when a tumor exists. So the S_{21} parameter, which depends on signal transmission and reception, can be used to represent the detection capability. If S_{21}^{inc} is the incident S parameter when there is no tumor inside the breast, S_{21}^{tot} is the total field S parameter when there is a tumor inside breast, the scatter S parameter S_{21}^{sct} is

$$S_{21}^{sct} = S_{21}^{tot} - S_{21}^{inc} \tag{1}$$

If no tumor exists, the antenna will only receive the background signals from the other. $|S_{11}|$ and $|S_{21}|$ in this condition are shown in Fig. 8 ($|S_{22}| = |S_{11}|$ and $|S_{12}| = |S_{21}|$ for the symmetric structure). $|S_{11}|$ still satisfies the requirements of the system, i.e., $|S_{11}| \leq -10\,\text{dB}$ between 2.7 and 5 GHz.

4.1. Case 1: Detection of a 10-mm Tumor at the Origin

Here, we connect the center points of two coaxial cable connectors of two opposite antennas, and define the center point of this line as origin (Fig. 7). First simulation case is assuming the 10-mm tumor (radius $r = 5\,\text{mm}$) is located at the origin ($x = 0\,\text{mm}$, $y = 0\,\text{mm}$, $z = 0\,\text{mm}$) as in Fig. 7. The horizontal distances (along z direction) between the tumor and both antennas are 50 mm.

Simulation results are shown in Fig. 9. The background field,

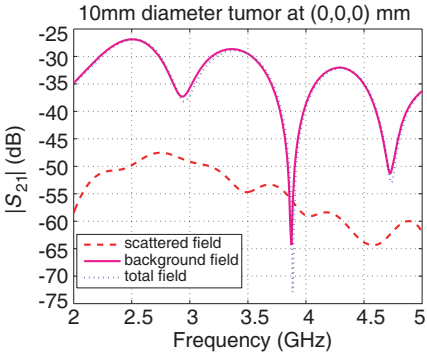

Figure 9. $|S_{21}|$ for the background field, incident field and scattered field when a 10-mm tumor is located at the origin.

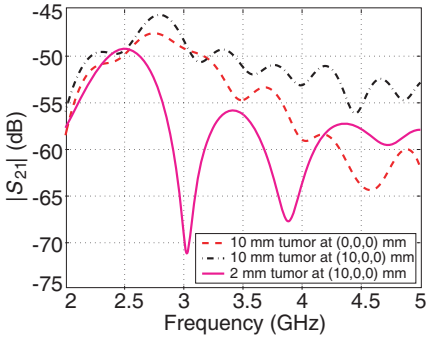

Figure 10. $|S_{21}|$ for the scattered field when a 10-mm tumor is located at $(0, 0, 0)$ mm and $(10, 0, 0)$ mm.

which is plotted by solid line, represents $|S_{21}^{inc}|$. The dotted line is total field ($|S_{21}^{tot}|$). The difference between these two lines are hard to see by eyes. So we subtract them according to Equation (1), and plot the magnitude of the subtraction results ($|S_{21}^{sct}|$) by dashed line. According to the experiences of [21, 22], the imaging system can detect and reconstruct the dielectric distribution of the object when $|S_{21}^{sct}|$ higher than -75 dB. Here, the simulated $|S_{21}^{sct}|$ ranges from -65 dB to -47 dB. So the antenna is suitable for the system to detect the tumors bigger than 10 mm in diameter.

4.2. Case 2: Detection of a 10-mm Tumor at $(10, 0, 0)$ mm

The origin is the deepest position in breast for antenna to detect (horizontally). However, there may be tumors located near the chest, for example at $(10, 0, 0)$ mm.

Simulation results are plotted in Fig. 10 by dotted line for a 10-mm tumor at $(10, 0, 0)$ mm. $|S_{21}^{sct}|$ for this tumor ranges from -56 dB to -45 dB. The position change of the tumor is detectable by the change of this $|S_{21}^{sct}|$.

4.3. Case 3: Detection of a 10-mm tumor at $(40, 0, 0)$ mm

In this case, the tumor is located closer to the chest (the open end of chamber) at $(40, 0, 0)$ mm. Simulation results are plotted in Fig. 10 by solid line. $|S_{21}^{sct}|$ for this tumor ranges from -52 dB to -80 dB. Scattered field of some frequencies are lower than -80 dB. But most

frequencies are detectable. And when antennas are mounted on the imaging chamber and build array, the performance will be better as discussed in the following Section 5.

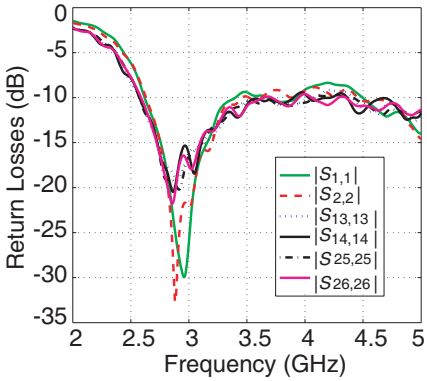

Figure 11. Return losses of 6 representative antennas in chamber.

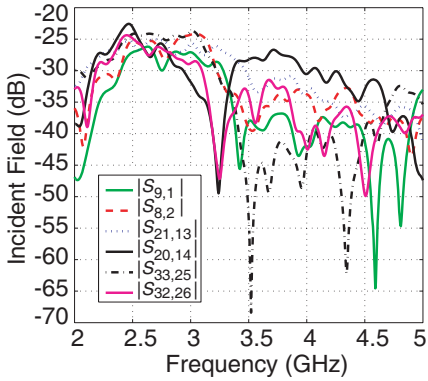

Figure 12. Incident field of 6 pairs of representative antennas in the imaging chamber.

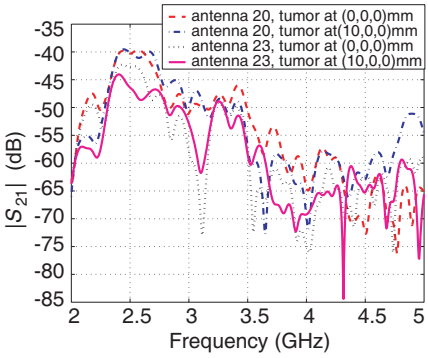

Figure 13. Scattered field results of antenna 20 and 23 as receivers, antenna 14 as transmitter on imaging chamber when a 10-mm tumor is located at origin and $(10, 0, 0)$ mm.

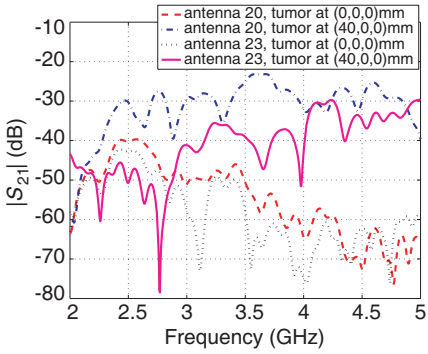

Figure 14. Scattered field results of antenna 20 and 23 as receivers, antenna 14 as transmitter on imaging chamber when a 10-mm tumor is located at origin and $(40, 0, 0)$ mm.

5. ANTENNAS ON CHAMBER

Antenna array design is another challenge for the imaging system. We modeled a simple prototype as Fig. 4 to validate the antennas performance when they are mounted on an imaging chamber. By the results of Section 3, vertical spacing of the antennas D_v is set to 17 mm. Although 5 mm horizontal spacing is enough for -20 dB isolation, we set $D_h = 20$ mm as a preliminary study of the antenna performance in chamber. The array is symmetric, so six antennas (center column and left column in Fig. 3(b)) are enough to represent the performance of all antennas. We choose antennas 1, 2, 13, 14, 25 and 26 as sources in the array shown in Fig. 4.

The return losses of these antennas are shown in Fig. 11. At the frequencies higher than 3.5 GHz, the return losses are slightly higher than -10 dB for part of the 6 representative antennas. Although antenna performance is slightly affected by the chamber, the antennas are still suitable for the imaging system.

Figure 12 plots the coupling of 6 pairs of antennas to their counterparts on the opposite side of the chamber. For example, antennas 1 and 9 are the antennas located in the upper left corner of two parallel walls of the chamber; the coupling result is shown as $|S_{9,1}|$ in Fig. 12; $|S_{33,25}|$ is for the pair located in the bottom corner of the chamber. The antennas are numbered in Fig. 4. These coupling results are simulated under the hypothesis that there is no tumor in the breast. So the results are the incident field. The magnitude of these incident fields are similar to the results simulated by two opposite antennas in Section 3.

Here we define the center point of the chamber as the origin; the x direction is pointed to the open face of the imaging chamber, and the y and z directions are pointed to two adjacent vertical walls. Similar to Section 3, we simulated and calculated the scattered field of a 10-mm tumor at three different positions, namely at the origin, $(10, 0, 0)$ mm, and $(40, 0, 0)$ mm. Fig. 13 and Fig. 14 show the different scattered field results at antenna 20 and 23 when antenna 14 is radiating. We can observe that the most scattered field is over -75 dB. This level of scattered field has been shown to enable imaging in a homogeneous fluid [8], although much more work needs to be done to allow imaging in a real breast tissue.

6. CONCLUSION

A simple half oval patch antenna is proposed for breast cancer imaging. Both simulation and measurement results show that the return loss of

the proposed antenna is less than −10 dB from 2.7 to 5 GHz. In a cubic imaging chamber, the antennas are mounted on four vertical walls. The couplings of two co-polarized antennas placed horizontally and vertically are studied for the antenna array design. And the detection capability of the antenna is simulated by two opposite antennas with 100 mm distance. The space between two antennas is filled with dielectric medium, which simply represents a model of breast immersed in perfect matching medium omitting the skin. Simulation results show that the antenna can detect the signal variation caused by a 10-mm tumor at different positions. According to the co-polarized coupling results, we modeled a chamber with $3 \times 3 \times 3$ antenna array. Simulation results prove that the proposed antenna is applicable to the breast cancer imaging system.

Ongoing work is being conducted to build appropriate antenna array, integrate them in the chamber, and perform experiments to validate the feasibility of the imaging system we proposed.

REFERENCES

1. Fear, E. C., S. C. Hagness, and P. M. Meaney, "Enhancing breast tumor detection with near-field imaging," *IEEE Microwave Mag.*, Vol. 3, No. 1, 48–56, 2002.
2. Fear, E. C. and M. A. Stuchly, "Microwave detection of breast cancer," *IEEE Trans. Microwave Theory Tech.*, Vol. 48, No. 11, 1854–1863, 2000.
3. Liu, Q. H., Z. Q. Zhang, T. Wang, G. Ybarra, L. W. Nolte, J. A. Bryan, and W. T. Joines, "Active microwave imaging I: 2-D forward and inverse scattering methods," *IEEE Trans. Microwave Theory Tech.*, Vol. 50, No. 1, 123–133, 2002.
4. Fear, E. C., P. M. Meaney, and M. A. Stuchly, "Microwaves for breast cancer detection," *IEEE Potentials*, Vol. 22, No. 1, 12–18, 2003.
5. Bindu, G., S. J. Abraham, A. Lonappan, V. Thomas, C. K. Aanandan, and K. T. Mathew, "Active microwave imaging for breast cancer detection," *Progress In Electromagnetics Research*, PIER 58, 149–169, 2006.
6. Zhang, H., S. Y. Tan, and H. S. Tan, "A novel method for microwave breast cancer detection," *Progress In Electromagnetics Research*, PIER 83, 413–434, 2008.
7. Zhang, Z. Q., Q. H. Liu, C. Xiao, E. Ward, G. Ybarra, and W. T. Joines, "Microwave breast imaging: 3-D forward scattering

simulation," *IEEE Trans. Biomed. Eng.*, Vol. 50, No. 10, 1180–1189, 2003.

8. Yu, C., M. Yuan, J. P. Stang, J. E. Bresslour, R. T. George, G. A. Ybarra, W. T. Joines, and Q. H. Liu, "Active microwave imaging II: 3-D system prototype and image reconstruction from experimental data," *IEEE Trans. Microwave Theory Tech.*, Vol. 56, No. 4, 991–1000, 2008.
9. Chen, G. P., Z. Q. Zhao, Z. P. Nie, and Q. H. Liu, "The prototype of microwave-induced thermo-acoustic tomography imaging by time reversal mirror," *Journal of Electromagnetic Waves and Applications*, Vol. 22, No. 11–12, 1565–1574, 2008.
10. Chen, G., Z. Zhao, Z. Nie, and Q. H. Liu, "Computational study of time reversal mirror technique for microwave-induced thermo-acoustic tomography," *Journal of Electromagnetic Waves and Applications*, Vol. 22, No. 16, 2191–2204, 2008.
11. Ybarra, G. A., Q. H. Liu, J. Stang, and W. T. Joines, "Microwave breast imaging," *Emerging Technologies in Breast Imaging and Mammography*, J. Suri, R. M. Rangayyan, and S. Laxminarayan (eds.), American Scientific Publishers, 2008.
12. Ybarra, G. A., Q. H. Liu, G. Ye, K. H. Lim, R. George, and W. T. Joines, "Breast imaging using electrical impedance tomography (EIT)," *Emerging Technologies in Breast Imaging and Mammography*, Ed.: J. Suri, R. M. Rangayyan, and S. Laxminarayan, American Scientific Publishers, 2008.
13. Ye, G., K. H. Lim, R. George, Jr., G. Ybarra, W. T. Joines, and Q. H. Liu, "3-D EIT for breast cancer imaging: System, measurements, and reconstruction," *Microwave Opt. Technol. Lett.*, Vol. 50, No. 12, 3261–3271, 2008.
14. Meaney, P. M., M. W. Fanning, D. Li, S. P. Poplack, and K. D. Paulsen, "A clinical prototype for active microwave imaging of the breast," *IEEE Trans. Microwave Theory Tech.*, Vol. 48, No. 11, 1841–1853, 2000.
15. Woten, D. A. and M. El-Shenawee, "Broadband dual linear polarized antenna for statistical detection of breast cancer," *IEEE Trans. Antennas Propag.*, Vol. 56, No. 11, 3576–3580, 2008.
16. Huang, W. and A. A. Kishk, "Compact dielectric resonator antenna for microwave breast cancer detection," *IET Microw. Antennas Propag.*, Vol. 3, No. 4, 638–44, 2009.
17. Jafari, H. M., J. M. Deen, S. Hranilovic, and N. K. Nikolova, "Co-polarised and cross-polarised antenna arrays for breast, cancer detection," *IET Microw. Antennas Propag.*, Vol. 1, No. 5, 1055–1058, 2007.

18. Yun, X., E. C. Fear, and R. H. Johnston, "Compact antenna for radar-based breast cancer detection," *IEEE Trans. Antennas Propag.*, Vol. 53, No. 8, 2374–2380, 2005.
19. Nilavalan, R., I. J. Craddock, A. Preece, J. Leendertz, and R. Benjamin, "Wideband microstrip patch antenna design for breast cancer tumour detection," *IET Microw. Antennas Propag.*, Vol. 1, No. 2, 277–281, 2007.
20. Bond, E. J., X. Li, S. C. Hagness, and B. D. Van Veen, "Microwave imaging via space-time beamforming for early detection of breast cancer," *IEEE Trans. Antennas Propag.*, Vol. 51, No. 8, 1690–705, 2003.
21. Yuan, M., C. Yu, J. P. Stang, R. T. George, G. A. Ybarra, W. T. Joines, and Q. H. Liu, "Experiments and simulations of an antenna array for biomedical microwave imaging applications," *URSI Meeting*, San Diego, CA, July 2008.
22. Stang, J. P., W. T. Joines, Q. H. Liu, R. T. George, G. A. Ybarra, M. Yuan, and I. Leonhardt, "A tapered microstrip patch antenna array for use in breast cancer screening via 3D active microwave imaging," *APS-URSI Meeting*, Charleston, SC, June 2009.
23. Jossinet, J. and M. Schmitt, "A review of parameters for the bioelectrical characterization of breast tissue," *Ann. N. Y. Acad Sci.*, Vol. 873, 30–41, 1999.
24. Woten, D. A., J. Lusth, and M. El-Shenawee, "Interpreting artificial neural networks for microwave detection of breast cancer," *IEEE Microwave Wireless Compon. Lett.*, Vol. 17, No. 12, 825–827, 2007.
25. Lazebnik, M., L. McCartney, D. Popovic, C. B. Watkins, M. J. Lindstrom, J. Harter, S. Sewall, A. Magliocco, J. H. Booske, M. Okoniewski, and S. C. Hagness, "A large-scale study of the ultrawideband microwave dielectric properties of normal breast tissue obtained from reduction surgeries," *Phys. Med. Biol.*, Vol. 52, 2637–2656, 2007.
26. Lazebnik, M., D. Popovic, L. McCartney, C. B. Watkins, M. J. Lindstrom, J. Harter, S. Sewall, T. Ogilvie, A. Magliocco, T. M. Breslin, W. Temple, D. Mew, J. H. Booske, M. Okoniewski, and S. C. Hagness, "A large-scale study of the ultrawideband microwave dielectric properties of normal, benign and malignant breast tissues obtained from cancer surgeries," *Phys. Med. Biol.*, Vol. 52, 6093–6115, 2007.